Orientation, Substructure, and Optical Properties of Rutile Films

V. M. Ievlev[a], K. A. Solntsev[b], S. A. Soldatenko[c], L. Yu. Leonova[a], P. V. Novikov[a], E. V. Golosov[d], A. A. Sinel'nikov[a], and A. M. Vozgor'kov[c]

[a] *Voronezh State University, Voronezh, 394006 Russia*

[b] *Baikov Institute of Metallurgy and Materials Science, Russian Academy of Sciences, Moscow, 119911 Russia*

[c] *Voronezh State Technical University, Voronezh, 394026 Russia*

[d] *Belgorod State University, Belgorod, 308015 Russia*

e-mail: aa_sinelnikov@mail.ru, rnileme@mail.ru

Abstract—The orientation, optical properties, and substructure of rutile films prepared by thermal and pulsed photon-assisted oxidation of single-crystal Ti films were investigated by transmission electron microscopy, optical spectroscopy, and high-energy electron diffraction. Crystallographic orientation relationships at the contact between titanium and rutile were established, and the energy band gap was determined. It was shown that the luminescence intensity decreased significantly with decreasing grain size from the submicrolevel to nanolevel.

Keywords: titanium, rutile, substructure, thin films, photoluminescence, transmittance spectra, oxidation, orientation.

INTRODUCTION

Numerous existing and potential uses for titanium dioxide are a major driving force behind the continuing development of new methods for preparing titania (anatase or rutile) of various morphologies (films, ceramics, powders, etc.) [1–5]. Most of the common synthetic techniques (wet-chemical deposition, magnetron sputtering, etc.) lead to formation of TiO_2 in the anatase form. As a result, the optical properties of this phase [6–10] and the changes occurring during the anatase–rutile transformation [11, 12] are well studied. In the present work, we aim to investigate the grain size effect on the photoluminescence of rutile thin films.

EXPERIMENTAL

Oriented rutile thin coatings were obtained by oxidation of corresponding epitaxial single-crystal titanium films [13]. This makes it possible to produce TiO_2 coatings of different orientation and substructure in a controlled and predictable manner.

Monocrystalline titanium thin films (50–60 nm) were deposited by the electron beam evaporation method on a synthetic mica (fluorine phlogopite) substrate chosen because of its high energy band gap value compared to rutile. The evaporation process was carried out at a substrate temperature of about 500°C under pressure below 10^{-4} Pa (oil-free pump).

The Ti films obtained were oxidized in open air either thermally (400, 600, or 1000°C for 10 min) or by photon-assisted oxide processing using high-power INP 16/250 pulsed xenon lamps.

The orientation and structure of synthesized titanium oxide films were studied using EMV-100BR and Tecnai G2 20F S-T transmission electron microscopes.

The transparency spectra of both TiO_2 thin films and thick (2–3 mm) polycrystalline samples obtained by prolonged oxidation of Ti specimens [14] were recorded in the range of 300–1950 nm on a Shimadzu UV-mini-1240 spectrophotometer. The luminescence properties were investigated within the wavelength range of 400–860 nm using a home-built spectrophotometer containing an MDR-4 monochromator (diffraction grating of 1200 lines/mm) and a pulsed LGI-21 UV laser (wavelength 337 nm, pulse duration 10 ns, pulse energy 3 μJ, pulse repetition frequency 100 Hz). The measurements were conducted in an optical cryostat immersed in liquid nitrogen (sample in vacuum).

RESULTS AND DISCUSSION

Figure 1 presents an electron diffraction pattern (a) and transmission electron microscopy (TEM) image (b) of titanium films vapor-deposited on the fluorine

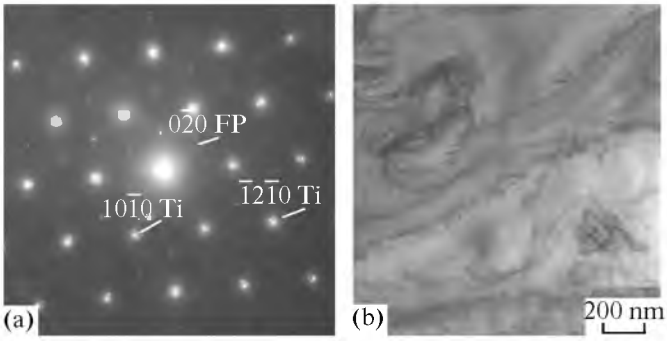

Fig. 1. (a) Electron diffraction pattern and (b) TEM images of Ti film deposited over synthetic mica (FP).

phlogopite substrate. As can be seen, monocrystalline Ti is oriented with respect to the substrate surface as

$$(0001), |11\bar{2}0|\mathrm{Ti} \parallel (001), [010]\mathrm{FP}. \quad (1)$$

The substructure of the films consists mostly of dislocations, dislocation clusters, and low-angle grain boundaries typical of uniformly oriented metal coatings [15].

Thermal Oxidation

We have shown previously [13] that thermal oxidation of oriented nanostructured Ti films in the temperature range of 300–400°C lead to formation of the epitaxial rutile phase growing through the entire thickness of titanium film owing to the active mutual diffusion along grain boundaries.

As can be seen from Fig. 2, the titanium dioxide (rutile) forms as an epitaxial film with the orientation relationships

$$(010), [100]\mathrm{TiO_2} \parallel (0001), [1\bar{1}00], [10\bar{1}0] \text{ and } [01\bar{1}0]\mathrm{Ti}. \quad (2)$$

Figure 2c demonstrates the scheme of conjugation of Ti and TiO_2 crystal lattices for all orientation relationships (2), including the twinning positions. The observed orientations can be explained via crystal packing analysis: a good fit between close-packed planes in the two crystal structures, high density of coincidence site lattice (CSL), small lattice mismatch, etc. [13, 15]. According to these crystallographic criteria, orientations (2) are optimal, while a three-dimen-

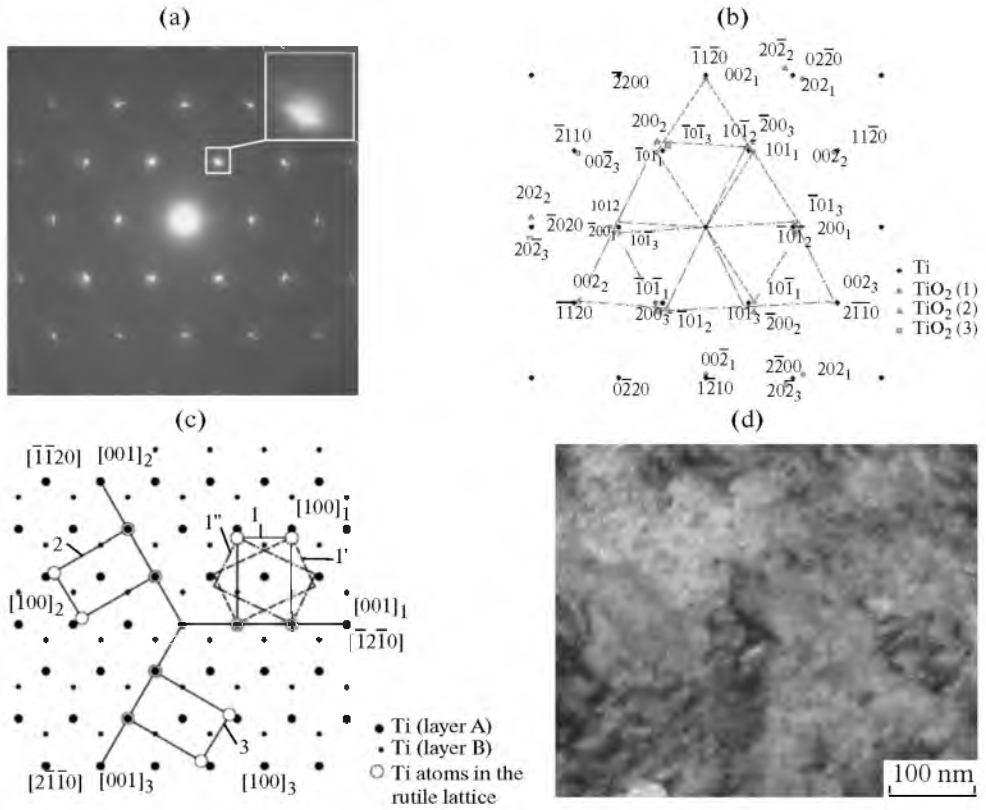

Fig. 2. (a) Electron diffraction pattern and (b) indexing scheme of Ti/TiO_2 film obtained by thermal oxidation at 400°C; (c) scheme of conjugation of Ti and TiO_2 crystal lattices for three equivalent azimuthal orientations 1, 2 and 3, where 1' is a twin plane of $(10\bar{1})$ and 1" is a twin plane of (101); (d) TEM image of Ti/TiO_2 film obtained by thermal oxidation at 400°C.

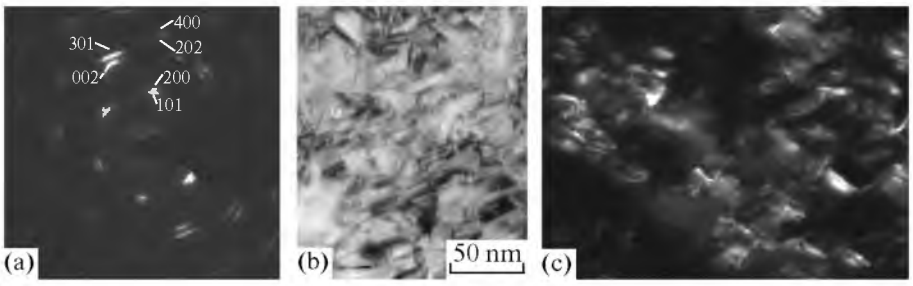

Fig. 3. (a) Electron diffraction pattern, (b) bright-field, and (c) dark-field TEM images of TiO_2 prepared by thermal oxidation procedure at 600°C.

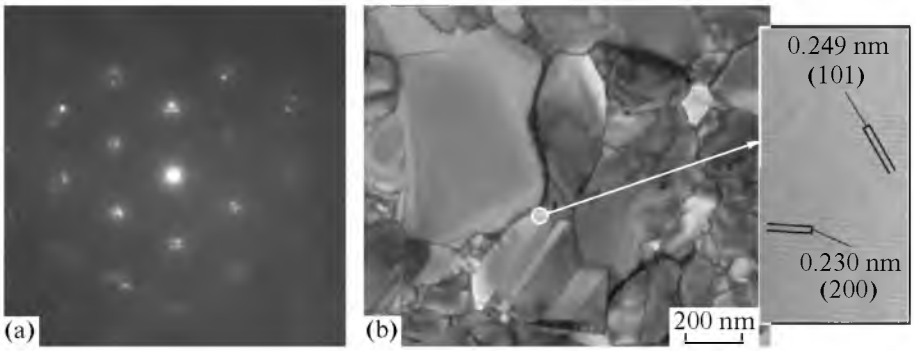

Fig. 4. (a) Electron diffraction pattern and (b) TEM images of rutile film prepared by thermal oxidation procedure at 1000°C.

sional lattice of coincident sites with the inverse ratio of coincidence sites to lattice sites ($\Sigma_1/\Sigma_2 = 4/2$ and basis vectors $\mathbf{A} = [100]TiO_2([1\bar{1}00]Ti)$, $\mathbf{B} = [010]TiO_2([0001]Ti)$, and $\mathbf{C} = [001]TiO_2([11\bar{2}0]Ti)$ provides the low-energy interphase boundary of TiO_2–Ti upon the conjugation of the low-index planes: $\{100\}$–$\{1\bar{1}00\}$, $\{010\}$–(0001), (001)–$(11\bar{2}0)$, $\{110\}$–$\{1\bar{1}02\}$, etc.

Annealing at 400°C for 10 min leads to formation of titanium dioxide with average grain size of 25 nm. The TEM image (bright-field mode) (Fig. 2d) revealed double diffraction of electron beams by the $\{11\bar{2}0\}$Ti and $\{002\}TiO_2$ planes within rutile grains. The resulting moiré pattern with a period of 88 nm or less (depending on the azimuthal disorientation angle and the operating Bragg reflections ($1\bar{1}00$ and 101, $1\bar{1}00$ and 200)) indicates, therefore, the presence of a two-layer heterostructure and that growth of TiO_2 film proceeds parallel to the titanium surface.

Figure 3 presents the electron diffraction pattern and both the dark- and bright-field TEM images of rutile film prepared by annealing at 600°C. As can be seen, the obtained oxide samples have a nanocrystalline substructure corresponding to orientations (2) with only a slight azimuthal disorientation of nanograins. Three symmetrically equivalent orientation relationships of the rutile and the possibility of twinning of crystals on $\{101\}$ planes lead to high dispersion of the film. The size of grains and subgrains determined from dark-field TEM images is about 30 nm, while high-resolution images taken at an accelerating voltage of 200 kV revealed blocks up to 150 nm in size. The main orientation relationships ((2) and twinning to it) in rutile film determine the formation of corresponding grains with high-angle 120 boundaries and $\{101\}$ twinning planes. It is known [17] that twinning on the $\{101\}$ rutile planes corresponds to a rotation around the $\langle 010\rangle$ axis by 117.2° (Fig. 2c). Therefore, the observed 120-degree grain boundaries can be regarded as a type of twin boundaries with misfit angle $\Delta\Theta$ of about 2.8°.

A further increase in the annealing temperature had no effect on either orientation relationships or azimuthal disorientation, leading only to some increase in grain size. Thus, the rutile films obtained at 1000°C were found to have the same orientations (2) and polycrystalline grain (50–500 nm) structure organized in blocks (Fig. 4).

Photon-Assisted Oxidation

Minimally, an irradiation energy E_I of 95 J/cm^2 and time of 1.2 s was required for complete oxidation of the Ti film to a rutile one. At the same time, increasing the exposure time and E_I to 2 s and 160 J/cm^2, respectively, resulted in no further significant structural or

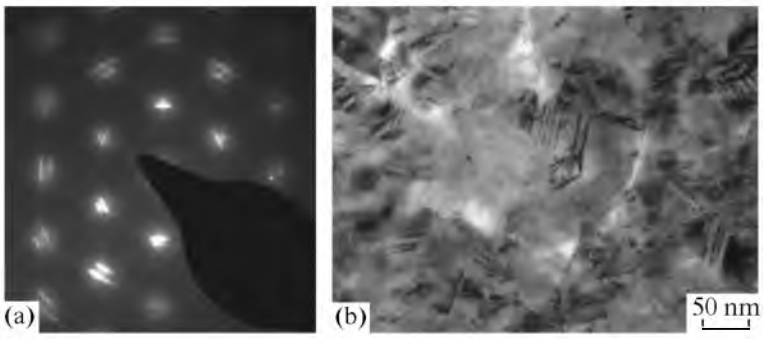

Fig. 5. (a) Electron diffraction pattern and (b) TEM images of rutile film prepared by photon-assisted oxidation procedure (E_I = 110 J/cm^2).

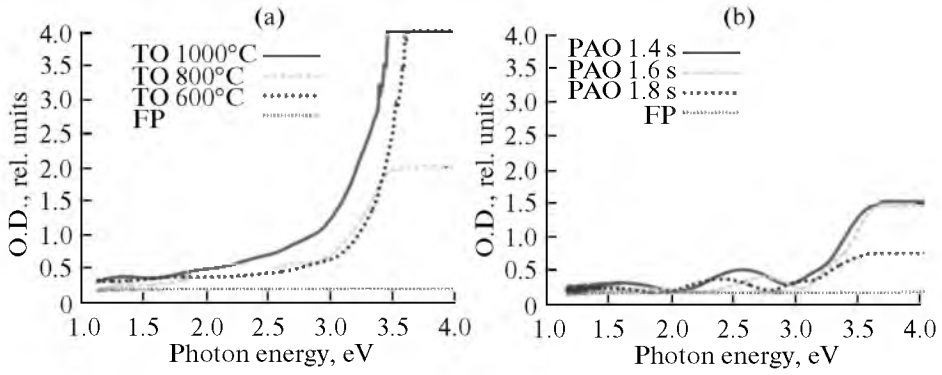

Fig. 6. Optical density spectra of rutile films on synthetic mica (FP) obtained by (a) thermal oxidation and (b) photon-assisted oxidation procedures.

phase transformations because of optical transparency of the newly formed rutile phase and fluorine phlogopite substrate.

Figure 5 presents the electron diffraction pattern and TEM image of a rutile thin film prepared by photon-assisted oxidation (E_I = 110 J/cm^2, 1.4 s). As can be seen, its orientation and structure are similar to ones observed in a sample prepared by the thermal oxidation procedure at 600°C (Fig. 3), while its grain substructure is more disperse and twinning positions are less represented.

Optical Properties

The transmittance spectra of TiO_2 films prepared by both thermal and photon-assisted oxidation on synthetic mica are given in Fig. 6. The observed rise in the optical density value at above 3 eV is attributed to interband indirect transitions of the rutile, while the peaks below it are the interference ones. The samples obtained at 400°C (thermal oxidation) or at an exposure time less than 1.2 s (photon-assisted oxidation) are optically opaque because of the presence of the metallic phase. Recorded spectra indicate the absence of impurity levels in the forbidden zone. The values of the width of the forbidden zone E_g for all studied samples are about the same (3.1 ± 0.2 eV); these values are close to the E_g value of monocrystalline rutile [18].

The luminescence spectra of TiO_2 films presented in Fig. 7 do not reveal any particular features in the visible wavelength region, but show the emission band at 820 nm typical of rutile. It should be noted that a 30-fold increase in intensity of this peak was observed for the sample synthesized at high temperature (Fig. 7a). Similar spectra were recorded for the bulk titanium dioxide samples obtained through treatment of massive Ti specimens at 875°C in air for 4 days (Fig. 7b). The intensity values of this emission band from samples synthesized through photon-assisted oxidation are comparable to one of the specimens prepared at 600°C by thermal oxidation (Fig. 7c).

Presumably, the near-infrared photoluminescence of rutile originates from luminescence centers at bulk defects of the crystal lattice. As was mentioned above, TiO_2 specimens prepared by annealing at 800 and 1000°C consist of large (500 nm) blocks, while the structure of samples obtained by photon-assisted oxide processing and by thermal oxidation at 600°C is composed of nanosized grains (below 30 nm). Owing to the size effects, such highly dispersed films have a

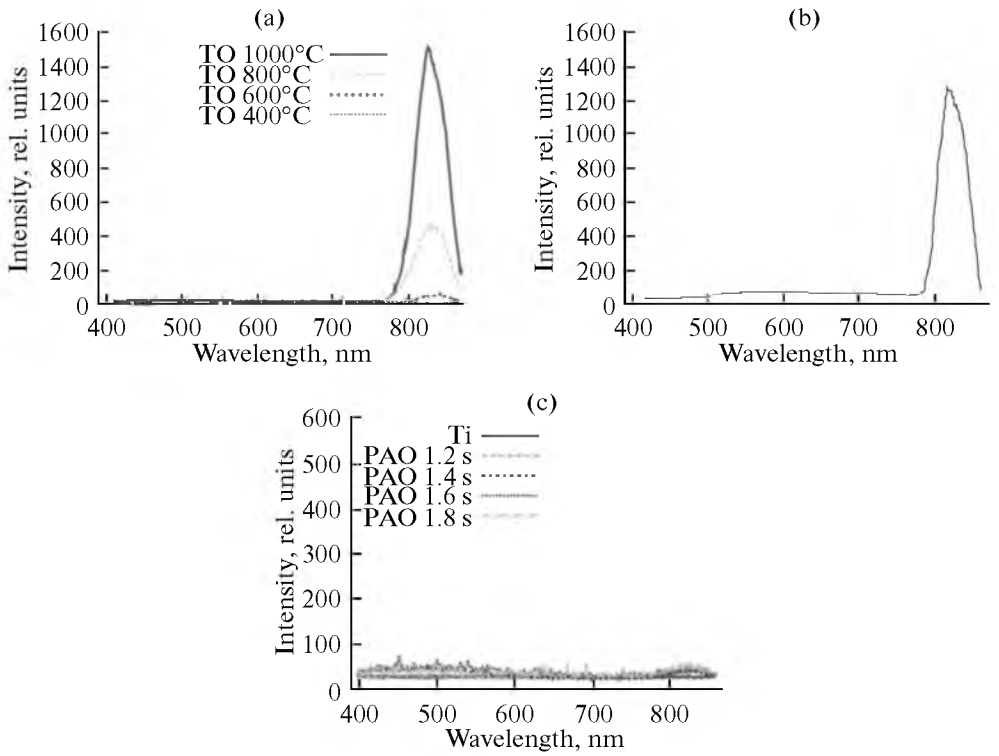

Fig. 7. Luminescence spectra (77 K) of rutile (a, c) thin films on synthetic mica (FP) and (b) bulk samples: (a, b) samples obtained by thermal oxidation; (c) samples obtained by photon-assisted oxidation.

low density of bulk defects, which results in a smaller radiative recombination probability in favor of nonradiative recombination at the grain and twin boundaries.

CONCLUSIONS

It was shown that photoluminescence of rutile thin films in the near-infrared region (~820 nm) decreases about 30-fold as their structure changes from submicrocrystalline to nanocrystalline.

ACKNOWLEDGMENTS

This work was supported by the federal target program "Human Capital for Science and Education in Innovative Russia" for 2009–2013 (project no. 02.740.11.0126).

REFERENCES

1. Hashimoto, K., Irie, H., and Fujishima, A., TiO_2 Photocatalysis: a Historical Overview and Future Prospects, *Jpn. J. Appl. Phys.*, 2005, vol. 44, no. 12, pp. 8269–8285.
2. Chong, L.H., Mallik, K., de Groot, C.H., and Kersting, R., The Structural and Electrical Properties of Thermally Grown TiO_2 Thin Films, *J. Phys. Condens. Matter*, 2006, vol. 18, pp. 645–657.
3. Luca, D. and Hsu, L.S., Structural Evolution and Optical Properties of TiO_2 Thin Films Prepared by Thermal Oxidation PLD Ti Films, *J. Optoelectron. Adv. Mater.*, 2003, vol. 5, no. 4, pp. 835–840.
4. Zhang, Y., Ma, X., Chen, P., and Yang, D., Crystallization Behaviors of TiO_2 Films Derived from Thermal Oxidation of Evaporated and Sputtered Titanium Films, *J. Alloys Comp.*, 2009, vol. 480, no. 2, pp. 938–941.
5. Wang, X., Feng, Zh., Shi, J., et al., Trap States and Carrier Dynamics of TiO_2 Studied by Photoluminescence Spectroscopy under Weak Excitation Condition, *Phys. Chem.*, 2010, No. 12, pp. 7083-7090.
6. Ghamsari, M.S. and Bahramian, A.R., High Transparent Sol–Gel Derived Nanostructured TiO_2 Thin Film, *Mater. Lett.*, 2008, vol. 62, pp. 361–364.
7. Wang, Z., Helmersson, U., and Käll, P.O., Optical Properties of Anatase TiO_2 Thin Films Prepared by Aqueous Sol–Gel Process at Low Temperature, *Thin Solid Films*, 2002, vol. 405, pp. 50–54.
8. Hasan, M.M., Haseeb, A.S., Saidur, R., and Masjuki, H.H., Effects of Annealing Treatment on Optical Properties of Anatase TiO_2 Thin Films, *Int. J. Chem. Biolog. Eng.*, 2008, Nos. 1–2, pp. 92–96.
9. Yang, C., Fan, H., Xi, Y., Chen, J., and Li, Z., Effects of Depositing Temperatures on Structure and Optical Properties of TiO_2 Film Deposited by Ion Beam Assisted Electron Beam Evaporation, *Appl. Surf. Sci.*, 2008, vol. 254, pp. 2685–2689.

10. Amor, S.B., Baud, G., Jacquet, M., and Pichon, N., Photoprotective Titania Coatings on PET Substrates, *Surf. Coat. Technol.*, 1998, vol. 102, pp. 63–72.

11. Won, D.-J., Wang, C.-H., Jang, H.-K., and Choi, D.-J., Effects of Thermally Induced Anatase-to-Rutile Phase Transition in MOCVD-Grown TiO_2 Films on Structural and Optical Properties, *Appl. Phys. A: Mater. Sci. Proc.*, 2001, vol. 73, no. 5, pp. 595–600.

12. Asthanaa, A., Shokuhfara, T., Gaoa, Q., et al., A Real Time Observation of Phase Transition of Anatase TiO_2 Nanotubes into Rutile Particles by in Situ Joule Heating inside Transmission Electron Microscope, *Microscopy and Microanalysis*, 2010, vol. 16, pp. 1360–1361.

13. Ievlev, V.M., Solntsev, K.A., Sinel'nikov, A.A., and Soldatenko, S.A., Orientation and Substructures of Hemoepitaxial Rutile Films, *Mater. Sci.*, 2010, No. 7, pp. 2–7.

14. Solntsev, K.A., Shustorovich, E.M., and Buslaev, Yu.A., Oxidative Constructing of Thin-Walled Ceramics (OCTC), *Dokl.-Chem.*, 2001, vol. 378, no. 4, pp. 143–149.

15. Ievlev, V.M., Bugakov, A.V., and Trofimov, V.I., *Rost i substruktura kondensirovannykh plenok: Uch. posobie* (Growth and Substructure of Condensed Films. A Tutorial), Voronezh: Voronezh. Gos. Tekhn. Univ., 2000.

16. Ashber, K.H.G., Smallman, R.E., and Williamson, G.K., Stacking Faults and Dislocations in Titanium Dioxide with Special Reference to Non-Stoichiometry, *Proc. Royal Soc. London, Ser. A: Math. Phys. Sci.,* 1963, vol. 276, no. 1367, pp. 542–552.

17. Belov, N.V., *Struktura ionnykh kristallov i metallicheskikh faz* (Structure of Ion Crystals and Metal Phases), Moscow: Akad. Nauk SSSR, 1947.

18. Daude, N., Gont, C., and Jonamin, C., Electronic Band Structure of TiO_2, *Phys. Rev., B: Solid State*, 1977, vol. 15, p. 3229–3235.